Wave-diffusion theory of spin transport in metals after ultrashort-pulse excitation

Steffen Kaltenborn,[1] Yao-Hui Zhu,[2] and Hans Christian Schneider[1,*]

[1]*Physics Department and Research Center OPTIMAS, University of Kaiserslautern, 67653 Kaiserslautern, Germany*

[2]*Physics Department, Beijing Technology and Business University, Beijing 100048, China*

(Received 18 November 2011; revised manuscript received 17 April 2012; published 1 June 2012)

Spin and charge-current dynamics after ultrafast spin-polarized excitation in a normal metal are studied theoretically using macroscopic wave-diffusion equations for spin-resolved carrier and current densities. It is shown analytically how this set of equations yields a unified description of ballistic and diffusive properties of spin and charge transport, including the intermediate regime between these two limits. In the framework of the wave-diffusion approach, ultrafast excitation of spin-polarized carriers in thin gold films is modeled assuming slightly spin-dependent momentum relaxation times along with standard parameters (Fermi velocity, spin and momentum relaxation times). The unified treatment of diffusive and ballistic transport yields robust signatures in the spin and charge dynamics that are in qualitative agreement with recent experimental results [Melnikov *et al.*, Phys. Rev. Lett. **107**, 076601 (2011)]. The influence of boundary effects on the temporal signatures of spin transport is also studied.

DOI: 10.1103/PhysRevB.85.235101 PACS number(s): 72.25.Ba, 73.23.Ad, 75.78.Jp, 85.75.−d

I. INTRODUCTION

Recent experimental research on spin dynamics in semiconductors, normal and ferromagnetic metals as well as half-metallic ferromagnets generally uses either "electronic" or optical excitation. In electronic setups, a spin current, a spin accumulation, or a precessing magnetization is driven by dc currents or microwave frequencies. Although optical techniques may be employed for the detection of spin-dependent phenomena, these techniques are used to measure transport characteristics at the frequencies associated with the excitation.[1,2] Purely optical techniques nowadays have the capability to excite and probe spin-dependent dynamics on timescales of several ten femtoseconds, and have shown how ultrafast spin-dependent dynamics take place. In particular, spin relaxation in semiconductors has been investigated,[3,4] lifetimes in metals have been measured,[5] and ultrafast changes of magnetic order by optical pulses have been discovered.[6,7]

Very recently there has been rapidly growing interest in studies that combine ultrafast optical excitation and detection with spin-transport phenomena. The ultrashort time scales involved in these studies entail combined dynamics of spin relaxation/scattering and transport. For instance, Oppeneer and coworkers have argued[8] that a superdiffusive transport process has an important influence on the measured magnetization dynamics in ferromagnets and electronic dynamics in metals, because transport processes already act *on the ultrafast timescales* on which the excited electrons are in nonequilibrium, or at least "hot." To obtain quantitative results on the influence of transport on "hot electrons," a recent experiment[9] excited spin-polarized carriers in an iron slab using an ultrashort laser pulse and probed the time-resolved spin and charge dynamics of the opposite side of an adjacent thin gold film using second-harmonic generation (SHG). This experimental setup made it possible to monitor charge and spin transport on length scales of about 100 nm and time scales of several ten femtoseconds after excitation with 35-fs pulses. Reference 9 provided a theoretical explanation of the spin-dependent transport dynamics based on the Fermi velocities of different carrier species (electrons and holes, spin-up and spin-down) that can be generated in the gold films. Depending on their mean-free paths (compared to the film thickness), it was argued that the different carrier species give rise to either predominantly ballistic or predominantly diffusive transport.

It is not easy to disentangle the effects of nonequilibrium relaxation and transport processes experimentally, because signatures of diffusive or ballistic transport already indicate the presence of scattering, or lack thereof. The present paper aims at a theoretical analysis of spin and charge transport after optical excitation in a macroscopic wave-diffusion model that can be derived from the Boltzmann transport equation. Importantly, this approach describes ballistic and diffusive transport regimes including the intermediate regime between the two "extreme" cases using a single set of equations for spin and charge transport. We thus do not need to make a distinction between predominantly ballistic or diffusive carriers as was done in Ref. 9. Because our approach is rooted in a close-to-equilibrium approximation it does not include *superdiffusive* transport processes, which result from an approximate treatment of pronounced nonequilibrium electronic dynamics.[8] Our approach compensates for this drawback by its numerical simplicity and robustness: it uses only three established parameters, i.e., Fermi velocity as well as momentum and spin relaxation times, which can be determined from transport measurements independently of the optical experiment.

In this paper, we use our approach to demonstrate the signatures of close-to-equilibrium transport on ultrashort timescales, in particular, in the region where neither a purely ballistic nor diffusive picture applies. In addition to the numerical results obtained from the macroscopic spin and charge transport equations, we provide an analytical discussion how both ballistic and diffusive transport are contained in these equations as special cases in the short-time and long-time limits. Since our theoretical approach contains ballistic and diffusive dynamics as special cases, it is well suited for a study of the behavior at the transition between ballistic and diffusive transport.

The paper is organized as follows. The time-dependent equation system, which forms the basis of our discussion is presented in Sec. II. Since this model was introduced in earlier papers,[10,11] we provide only a brief explanation of the macroscopic dynamical equations. In Sec. III, we show analytically how the wave character of these equations is related to ballistic transport. In Sec. IV B, we present numerical results for the spin and charge dynamics in a gold film after spin-polarized optical excitation and compare our results to recent experiments. We summarize our results in Sec. V.

II. TIME-DEPENDENT EQUATION SYSTEM

For a macroscopic description of spin currents and the accompanying spin accumulation at the boundaries of multilayer systems, one often applies macroscopic spin-diffusion theory.[4,12–16] The infinite propagation velocity for spin (and charge) signals inherent in this approach becomes troublesome at high frequencies and/or switching speeds, and can be circumvented by using the macroscopic spin *wave-diffusion* equations, which form the basis of the theoretical analysis in this paper. Their derivation together with applications to collinear and noncollinear spin transport has been discussed in Refs. 10 and 11. These papers also contain relevant citations for the derivations of the equations.

The basic quantities in this approach are the macroscopic spin-current density $J_s(z,t)$ and spin density $n_s(z,t)$ of conduction electrons in parabolic bands with spin projection quantum number $s = \pm 1/2$. The densities obey the dynamical equations

$$\frac{\partial J_s(z,t)}{\partial z} + \frac{\partial n_s(z,t)}{\partial t} = -\frac{n_s(z,t) - n_{-s}(z,t)}{\tau_{\mathrm{sf}}}, \tag{1}$$

$$\frac{J_s(z,t)}{\tau_s} = -c_{\mathrm{sig}}^2 \frac{\partial n_s(z,t)}{\partial z} - \frac{\partial J_s(z,t)}{\partial t}. \tag{2}$$

While the continuity equation (1) is the same as in macroscopic spin-diffusion theory,[4,12] Eq. (2) is a time-dependent generalization of Fick's law, where the time derivative $\partial J_s/\partial t$ describes relaxation processes in addition to the "diffusive" space derivative $\partial n_s/\partial z$. For the description of multilayers, it is assumed that the same bands with spin label s exist in each part of the heterostructure. Further, τ_{sf} and τ_s are the spin flip and the (spin-dependent) momentum relaxation times that result from quasiequilibrium averages over electronic distributions.

In ferromagnets, the momentum relaxation times τ_s are different for majority and minority electrons, but in nonmagnetic metals they are spin independent close to equilibrium, i.e., $\tau_s = \tau_{-s}$. Nonequilibrium spin-dependent excitation in normal metals on short timescales does lead to spin-dependent lifetimes. We therefore assume different momentum relaxation-times $\tau_s \neq \tau_{-s}$ for normal metals after spin-dependent excitation in this paper. Regardless of the excitation conditions, spin-dependent momentum relaxation times may also arise in an experiment, such as the one in Ref. 9, if an external field for the measurement of magneto-optical signals is applied.

To make this paper more self-contained, we collect some results from Ref. 10: there it was shown that an important consequence of the macroscopic wave-diffusion equations is the occurrence of the spin-signal-propagation velocity,

$$c_{\mathrm{sig}} = \frac{v_{\mathrm{F}}}{\sqrt{3}}, \tag{3}$$

where v_{F} is the Fermi velocity. Equations (1) and (2) can be combined to yield a wave-diffusion equation[10] for the total spin density $n_m = n_+ - n_-$,

$$\frac{\partial^2 n_m}{dt^2} + \left(\frac{1}{\tau} + \frac{1}{T_1}\right)\frac{\partial n_m}{dt} + \frac{n_m}{\tau T_1} = c_{\mathrm{sig}}^2 \frac{\partial^2 n_m}{dz^2}, \tag{4}$$

where $T_1 = \tau_{\mathrm{sf}}/2$ is the spin-relaxation time and τ the "average" momentum relaxation time. The equation above contains a second-order time derivative, which is absent in the spin diffusion equation.[4] This additional term shows that it takes a finite time for the spin current to adjust to the gradient of the spin accumulation.[17,18] The second-order time and space derivatives lead to a wave character of the dynamical spin and charge transport in addition to its diffusive character and that time-dependent macroscopic spin transport shows wavelike and diffusive properties. From this viewpoint, the time-dependent spin diffusion equation can be regarded as an approximation of the wave-diffusion behavior in the long-time/low-frequency limit.

III. BALLISTIC AND DIFFUSIVE TRANSPORT FROM THE WAVE-DIFFUSION EQUATION

In this section, we connect the wave-diffusion equation (4) with diffusive and ballistic behavior of spin transport. To this end, we analyze the spatiotemporal behavior of a spin-polarized carrier distribution that is initially concentrated at $z = 0$, i.e., the initial condition

$$n_m(z,0) = N_m \delta(z). \tag{5}$$

To this end, we calculate the mean-square displacement[19]

$$\Delta_z^2(t) = \frac{1}{N_m}\int_{-\infty}^{\infty} z^2 n_m(z,t)\, dz \tag{6}$$

with $N_m = \int_{-\infty}^{\infty} dz\, n_m(z,0)$. We will interpret $\Delta_z^2(t) - \Delta_z^2(0) \propto t^2$ as ballistic and $\Delta_z^2(t) - \Delta_z^2(0) \propto t$ as diffusive transport in accordance with electronic wave packet dynamics. Note that we have $\Delta_z^2(t=0) = 0$.

We now construct a solution of the wave-diffusion equation with the initial condition (5) using damped dispersive solutions of the form

$$n_m \propto e^{i(kz-\omega t)} \tag{7}$$

as done by Weiss[20] for transport equations resulting from persistent random walk models.

To determine the temporal damping characteristics of n_m, we let $\omega(k)$ become a complex function of the wave vector. This should be contrasted with Ref. 10 where $k(\omega) = k_{\mathrm{R}}(\omega) + ik_{\mathrm{I}}(\omega)$ was chosen as a complex quantity to obtain the damping length as a function of frequency. Substituting Eq. (7) into Eq. (4), we get the dispersion relation

$$-\omega^2 - i\alpha\omega + \xi = -c_{\mathrm{sig}}^2 k^2, \tag{8}$$

where $\alpha = \frac{1}{\tau} + \frac{1}{T_1}$ and $\xi = \frac{1}{\tau T_1}$. We obtain two purely imaginary solutions $\omega_\pm = -i\gamma_\pm$ with

$$\gamma_\pm(k) = \frac{1}{2}\left(\frac{1}{\tau} + \frac{1}{T_1}\right) \pm \frac{1}{2}\sqrt{\left(\frac{1}{\tau} + \frac{1}{T_1}\right)^2 - 4\left(\frac{1}{\tau T_1} + c_{\mathrm{sig}}^2 k^2\right)}, \tag{9}$$

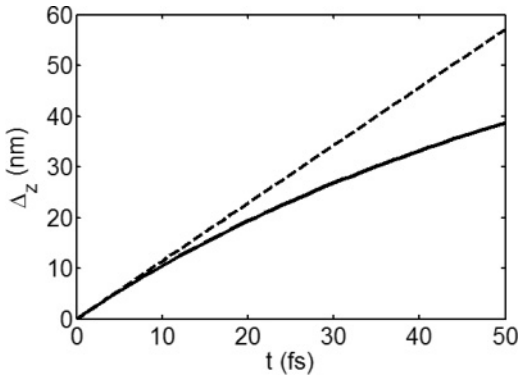

FIG. 1. Mean-square displacement $\Delta_z(t)$ of the spin density vs. time: transition from ballistic to diffusive spin transport.

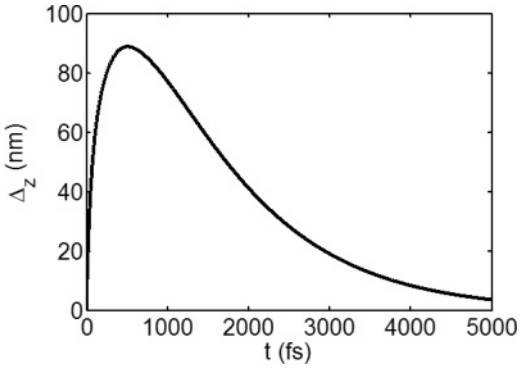

FIG. 2. Same as Fig. 1 on a longer time scale.

which describe an exponential decay of $n_m(z,t)$ and $J_m(z,t)$ in time. The initial condition (5) can now be satisfied by the Fourier integral

$$n_m(z,t) = N_m \int_{-\infty}^{\infty} \frac{dk}{2\pi} e^{ikz}[e^{-i\omega_+(k)t} + e^{-i\omega_-(k)t}], \quad (10)$$

from which one reads off the Fourier transformed density

$$\begin{aligned}\tilde{n}_m(k,t) &= N_m \int_{-\infty}^{\infty} dz e^{-ikz} n_m(z,t) \\ &= N_m[e^{-\gamma_+(k)t} + e^{-\gamma_-(k)t}]. \end{aligned} \quad (11)$$

The mean-square displacement can be expressed with the help of the second derivative of the Fourier transformation and explicitly evaluated as follows:

$$\begin{aligned}\Delta_z^2(t) &= -\frac{1}{N_m} \left.\frac{\partial^2 \tilde{n}_m(k,t)}{\partial k^2}\right|_{k=0} \\ &= \frac{2c_{\rm sig}^2 t}{\left(\frac{1}{\tau} - \frac{1}{T_1}\right)}(e^{-t/T_1} - e^{-t/\tau}), \end{aligned} \quad (12)$$

where we assumed $\tau < T_1$. Equation (12) describes the behavior of $\Delta_z^2(t)$ for all times.

In Fig. 1, we plot the time dependence of the mean-square displacement for the parameters $(\tau, T_1, c_{\rm sig})$ of gold (see Sec. IV A). On time scales for which the spin relaxation is not important, i.e., $t < T_1$, Eq. (12) simplifies to

$$\Delta_z^2(t) \simeq 2c_{\rm sig}^2 t\tau(1 - e^{-t/\tau}). \quad (13)$$

For short times, $t \ll \tau$, we have $\Delta_z^2(t) \propto c_{\rm sig}^2 t^2$. The characteristic ballistic behavior of Δ_z^2 is consistent with the limit $t \ll \tau$, which describes a time scale shorter than typical (momentum) relaxation processes. For times on the order of the momentum relaxation time τ, momentum scattering processes come into play, and the ballistic behavior is gradually lost. More precisely, for $\tau < t < T_1$, the behavior of the second moment is $\Delta_z^2(t) \propto c_{\rm sig}^2 \tau\, t$ with corrections of the order $\exp(-t/\tau)$. By virtue of $c_{\rm sig}^2 \tau = D$ and disregarding exponentially small corrections, this means $\Delta_z^2(t) \propto Dt$, which is a signature of diffusive transport with diffusion constant D. Finally, for times on the order of (and longer than) the spin relaxation time T_1, we have an exponential decay of $n_m(z,t)$ and also an exponential decay of $\Delta_z^2(t)$ (see Fig. 2). This result is simply a consequence of the relaxation of the spin polarization due to spin-flip processes. These considerations clarify how the macroscopic wave-diffusion equations (1) and (2) are capable of describing both the ballistic and diffusive properties of spin transport as well as the transition between the two limits. We will use these concepts in the discussion of the numerical results for spin transport after ultrashort optical excitation in the following section.

IV. NUMERICAL RESULTS

A. Model and computational setup

In this section, the time-dependent equation system presented in Sec. II is applied to a model setup that aims at analyzing the spin and charge transport as it occurs in the experiment of Melnikov *et al.*[9] as shown in Fig. 3. In the experiment, spin-polarized carriers are excited optically by a 35-fs pump pulse in a Fe/Au slab structure. The excited carriers propagate from the iron into the adjacent nonmagnetic gold slab, and the charge and spin dynamics at the right gold surface are extracted from the time-dependent magneto-optical response at the gold surface.

The excitation of nonequilibrium carriers by ultrashort pulses across interfaces and junctions poses challenging problems for microscopic theories, see, e.g., Refs. 21–24. For the Fe/Au interface, Ref. 9 analyzed in some detail the band lineup of Fe and Au, and used energy and momentum conservation to determine the type of carriers that can be generated in the Au film by excitation in the Fe layer. For the purpose of the present paper, namely, the determination of the space- and time-resolved spin and charge dynamics in the gold layer, we use a simplified view of the excitation process across the Fe/Au interface: photoexcited carriers in the Fe generate a spin-polarized current that is carried by the same

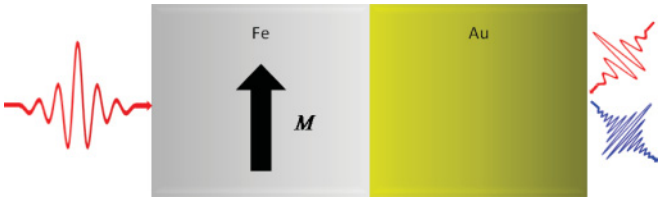

FIG. 3. (Color online) Schematic setup of the optical pump-probe experiment on a Fe/Au heterostructure.

type of charge carriers, usually assumed to be s electrons, through the whole multilayer structure. This assumption also underlies the derivation of the macroscopic diffusion and wave-diffusion equations.[10,12] Technically, we introduce the following simplifications. First, we assume that the spin signal excited in the iron layer can be modeled as a boundary value for the spin and charge densities in the adjacent gold slab. Second, we neglect the spin and charge transport of holes. We then use the macroscopic equations for the electron densities, $n_s(z,t)$, and current densities, $J_s(z,t)$, in the spin-up and spin-down bands, respectively, of a ferromagnet-metal heterostructure. These dynamical macroscopic equations can be derived from the Boltzmann transport equation for the microscopic carrier distributions under the assumption that the deviations from an equilibrium distribution around the Fermi surface are small.[10] We therefore use the following simplified view of the complicated injection and relaxation process: spin-polarized carriers are created in the iron layer and move into the spin-degenerate gold bands where this is allowed in the band structure. We assume a very fast initial electronic energy equilibration, so that we have quasiequilibrium distributions in the spin degenerate bands in gold, but with different densities. The momentum relaxation times of the quasi-equilibrium electrons of different spin, τ_+ and τ_-, which arise microscopically from averages over the energy dependence of the electronic distributions, should then also be different. We therefore treat the difference of the relaxation times, τ_+ and τ_-, as a parameter that needs to be specified. In addition, we could also treat the spin polarization of the injected electrons as a parameter, but we choose not to do so to avoid the introduction of fit parameters. Since it turns out that the dependence of our results on the difference of momentum relaxation times is extremely weak, the only important parameters of our macroscopic equations have values that are well established from electrical transport measurements: the Fermi velocity v_F, the momentum relaxation time τ_s and the spin relaxation time T_1. Using our approach thus yields the dynamics due to quasiequilibrium transport, and can be compared to more involved treatments of the relaxation processes away from the Fermi energy. For instance, these relaxation processes may lead to superdiffusive transport.[8]

In order to solve Eqs. (1) and (2) numerically for electronic transport in the gold layer, we need the boundary condition at the interface to the ferromagnet, i.e., the left boundary of our computational domain, which we take to be $z = 0$. For simplicity, we assume that the spin-current density as a function of time is known at the Fe/Au interface. This approximation neglects the spin current flowing back to the iron layer due to the spin accumulation in the gold layer. At the Fe/Au interface, $z = 0$, the spin-current density is assumed to be a Gaussian

$$J_s(z = 0,t) = J^0 e^{-t^2/t_0^2}, \tag{14}$$

where $t_0 = t_{\mathrm{FWHM}}/(2\log 2)$, and J^0 is the maximum current density. Note that we assume the same initial condition for the currents in the minority and majority channel. We choose $t_{\mathrm{FWHM}} = 35$ fs as full width at half maximum of the current pulse, which is the duration of the exciting laser pulse in the experiment, and $J^0 = 10^{-4}$ nm^{-2}fs^{-1}. For the Au layer, we choose a momentum relaxation time of $\tau_p = 30$ fs (from Ref. 25) and $c_{\mathrm{sig}} = 0.808$ nm/fs ($v_F = 1.4$ nm/fs, see Ref. 26). The spin relaxation time $T_1 = 515$ fs is determined from the spin-diffusion length[27] $l_{\mathrm{sf}} = 100$ nm via the identity[10,12] $l_{\mathrm{sf}} = c_{\mathrm{sig}}\sqrt{\tau_p T_1}$. The resulting electron mean-free path is $\lambda = v_F\tau_p = 42$ nm.

In the following, we take the literature value of the momentum relaxation-time for one spin channel, i.e., $\tau_+ = \tau_p$, but $\tau_- \neq \tau_+$ to mimic the effect of different microscopic distribution for majority and minority electrons that propagate into the gold layer. Some justification for our approximation is provided by the weak dependence of the numerical results on the actual value chosen for τ_-.

We study two simplified variations of the setup depicted in Fig. 3. In the first case, we assume an "infinitely thick" gold layer to avoid the influence of the reflected spin signal. In this case, we assume that the thickness L of the gold slab is so large that spin and charge signals have not propagated to the right boundary during the time interval of interest, i.e., $L \gg l_{\mathrm{sf}}$. In this time frame, the choice of the boundary condition at the right of the gold layer does not influence the results. For computational convenience, we require both spin-(charge-) current and spin (charge) densities to be zero. We also study the case of a finite thickness L of the gold layer. Here, we require the spin and charge current densities to vanish at the right boundary of the gold layer. Although it may seem that this boundary condition applies to the experiment best, it leads to multiple reflections that do not show up in the experiment, as is discussed in more detail below. The numerical solution of Eqs. (1) and (2) employs the method of characteristics as detailed in Ref. 10.

B. Spin and charge dynamics

We first discuss results for the time evolution of the spin and charge density in an "infinitely thick" layer. Fig. 4(a) shows the spin density $n_+(z = z_0,t)$ for majority electrons at different positions $z = z_0$, ranging from $z_0 = 25$ to 150 nm. As mentioned above, the results at position $z = z_0$ mimic the dynamics at the surface for a slab thickness L. We find a delayed sharp rise and a peak in the carrier density. We first discuss the curve for $z_0 = 25$ nm in Fig. 4(a), which is in the regime where ballistic transport properties are dominant, as shown by Fig. 1. The pronounced peak occurs at time $t_{\mathrm{peak}} = z_0/c = 34$ fs, and therefore is related to wave-like propagation dynamics, which corresponds to ballistic transport as shown in Sec. III. Further, the wavelike dynamics of the carrier distribution preserves to some extent of the Gaussian shape of the driving current pulse $J_s(z = 0,t)$, which is created by the drive current at the left boundary. The difference between the full and the purely ballistic result is, of course, due to momentum and spin-flip scattering. These contributions lead to an asymmetric peak and the slow decay, but not to a broadening of the peak. This can be seen by comparing with the result for an infinitely thin layer (not shown), in which the dynamics are completely ballistic. For peaks at larger distances (and longer times), the peaklike signature is gradually lost as one reaches the regime where the diffusive behavior becomes dominant, and the ballistic (wavelike) component is essentially only seen in the delayed onset of the signal.

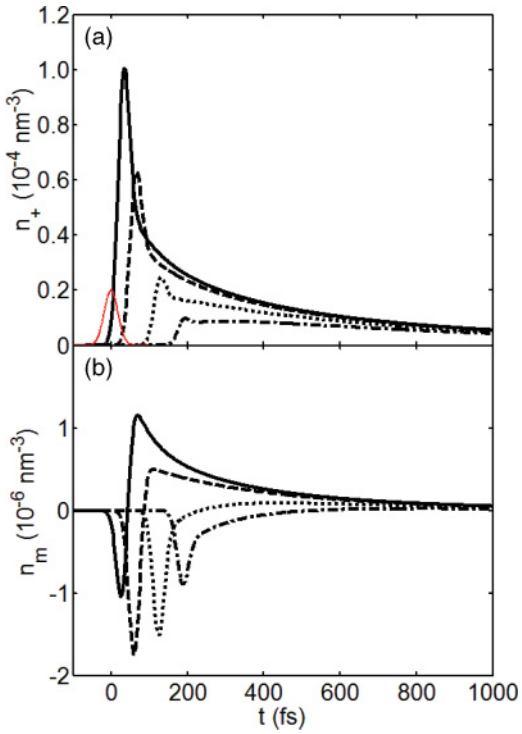

FIG. 4. (Color online) Time evolution of the density $n_+(z_0,t)$ of majority electrons (a) and the total spin density $n_m(z_0,t)$ (b) at positions $z_0 = 25$ (solid), 50 (dashed), 100 (dotted), and 150 nm (dash-dotted) of an infinitely thick layer. The excitation current pulse J_s is also shown in arbitrary units (thin red line).

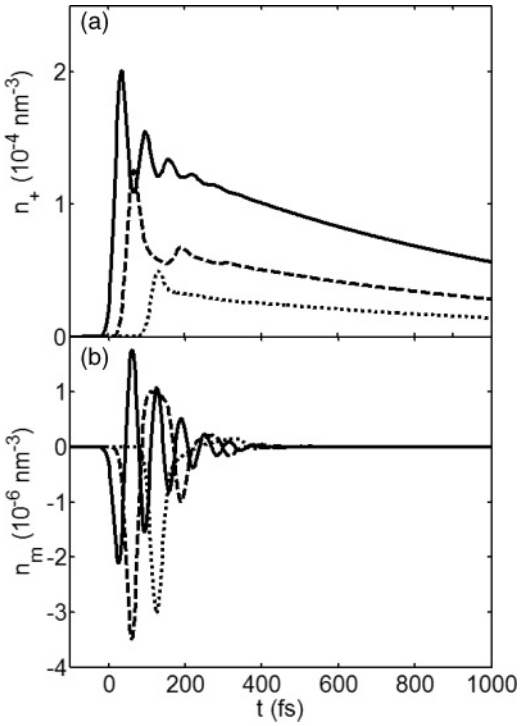

FIG. 5. Time evolution of the spin density of majority electrons $n_+(z = L,t)$ (a) and the total spin density $n_m(z = L,t)$ (b) for Au layer thicknesses of $L = 25$ (solid), 50 (dashed), and 100 nm (dotted).

We therefore interpret the dynamics in Fig. 4(a) as ballistic for short times, as more or less diffusive for "intermediate" times, and eventually as an exponential decay for long times. From the ballistic motion of electrons traveling with v_F in a straight line towards the opposite surface, one may naively expect the arrival of a signal with the Fermi velocity instead of $c_{sig} = v_F/\sqrt{3}$. This is only true for carriers "going straight" to the opposite surface, and these carriers are responsible for the onset of the signal. The occurence of the peak with a smaller velocity as well as the finite width of the peak shows that there is a spread in the time the carriers need to traverse a fixed distance in z direction.

The curve for minority electrons $n_-(z_0,t)$ (not shown) is almost indistinguishable from the one shown for $n_+(z_0,t)$ on the scale of Fig. 4(a) if we choose the same excitation, i.e., boundary condition, and change the momentum relaxation time for "−" electrons by 5% to $\tau_- = 31.5$ fs. However, as Fig. 4(b) shows, the total spin density $n_m(z_0,t) = n_+(z_0,t) - n_-(z_0,t)$ is influenced quite drastically by this change. Qualitatively, this can be understood by considering the following picture of the dynamics of individual electrons, even though the calculation deals with distribution functions and the momentum relaxation times are for ensemble averages only; the longer momentum relaxation time results in the minority electrons arriving earlier than the majority ones, which causes a characteristic shape of the spin dynamics with a negative spike in the spin density. When the majority electrons arrive, the signal of the minority carriers already falls off. Therefore the spin density n_m changes sign and only afterwards shows a long positive tail. Importantly, the difference between the momentum relaxation times can be changed from 1% to 100% leading to changes in the numerical values of the spin density, but not in the qualitative behavior. Thus as long as there is a difference between τ_+ and τ_-, the resulting shape of the spin dynamics with the characteristic short negative dip and a long positive decay is extremely robust.

We now discuss the results for the case in which the finite thickness L of the metal layer is modeled by a boundary condition for $n_s(z,t)$ at $z = L$. Figure 5(a) shows the spin density $n_+(z = L,t)$ for majority electrons at the right boundary of the gold slab as a function of time for slab thicknesses $L = 25$, 50, and 100 nm, respectively.[28] Several oscillations are visible for the 25-nm slab. For the 50-nm slab, only a second peak occurs before the signal decays. This happens because, unlike the case in Fig. 4(a), the electrons are reflected at the right metal surface and continue to propagate/diffuse through the slab. Depending on the thickness of the layer, they may be reflected also at the left boundary, i.e., the Fe/Au interface in the experiment, and propagate again to the right metal boundary. This behavior continues as long as there is a ballistic component to the dynamics and vanishes when the dynamics become diffusive. Eventually, the signal decays on the time scale of the spin relaxation time. In the 100 nm thick layer, in particular, the ballistic character is further reduced, so that no additional peaks develop at all. The additional peaks, if present in the density dynamics n_+ of one spin channel, are also visible in the total spin-density dynamics, n_m, as shown in Fig. 5(b). Depending on the thickness of the layer, the spin signal can change sign more than once for the same reason as without reflection because the propagation and reflection dynamics

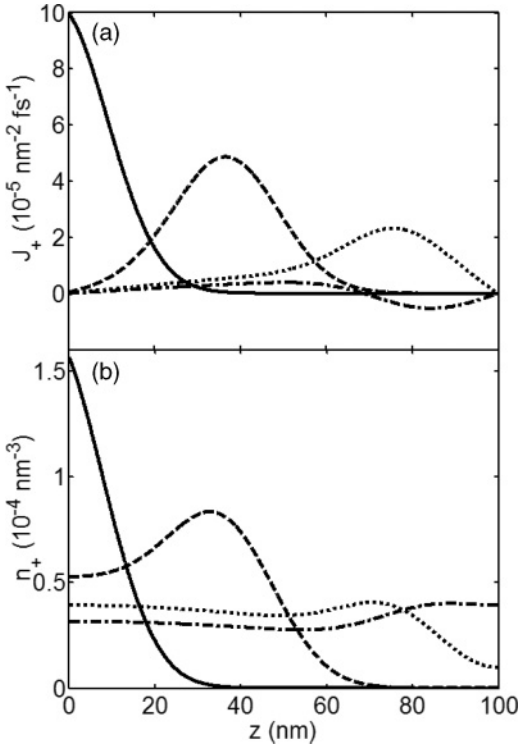

FIG. 6. Snapshots of the spin-current density $J_+(z,t)$ (a) and of the spin density $n_+(z,t)$ (b) as a function of z at times $t = 0$, 50, 100, and 150 fs for a 100-nm gold slab.

occurs for both spins with a slightly different relaxation time, so that the maxima and minima of n_- are slightly shifted with respect to those of n_+.

Figure 6 shows the space dependence of the current and density distributions for "+" electrons for a slab of thickness $L = 100$ nm at different times. The snapshots of the current density, Fig. 6(a) show how the initial current pulse propagates through the gold slab, is attenuated, and changes sign after it reaches the right slab boundary. The sign change indicates that the propagation direction of the carriers is reversed, i.e., carriers moving ballistically are reflected when they reach the boundary. This is another indicator that even in the case of the 100-nm gold slab, the ballistic character of the transport is still recognizable at the surface. The spin density $n_+(z,t)$, shown in Fig. 6(b), exhibits a wave front at first and a subsequent "smoothing" out due to the diffusive character of the dynamics, which becomes dominant after a few hundred femtoseconds.

Finally, Fig. 7 shows the time evolution of the charge density $n(z = L,t)$ at the right boundary of the gold slab for slab thicknesses $L = 25$, 50, 100, and 150 nm, respectively. Dependent on the thickness, there are additional peaks due to multiple reflections on the boundaries and charge accumulation in the gold layer. The charge accumulates and reaches a steady state because we neglect a possible flowing back of the charge-current into the iron layer. In an infinitely thick gold layer, the Gaussian current pulse, which mimics the excitation, propagates through the nonmagnetic gold while its maximum decays. Thus the space-resolved results for the spin and charge

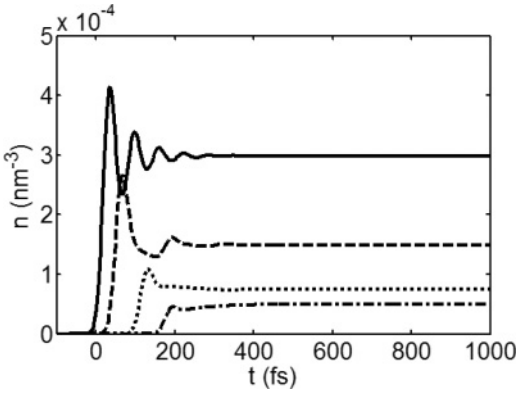

FIG. 7. Time evolution of the charge density $n(z,t)$ for layer thicknesses of $L = 25$ (solid), 50 (dashed), 100 (dotted), and 150 nm (dash-dotted line).

dynamics show that there is no spin and charge accumulation in an infinitely thick gold layer.

C. Relation to experiment

We have already described the idea of the experiment by Melnikov *et al.*, and our calculation applies to the basic setup of that experiment, as shown in Fig. 3. Although we do not calculate the electric fields generated by second-harmonic effects at the back surface as measured in the experiment, we follow the interpretation of the experimental results by Melnikov *et al.*, and compare the "charge" signal with the charge density n and the "magnetic" signal with n_m. An important experimental finding is a fast rise and a subsequent slow decay of the charge signal accompanied by a magnetic signal that shows a characteristic sign change. Comparing the spin density n_m at the right boundary for slab thicknesses 50 and 100 nm, see Fig. 4(b), with the *magnetic* SHG signal shown in Figs. 2(c) and 2(d) of Ref. 9 one finds a qualitative agreement. In particular, the time at which the sign change of the signal occurs and the decay at longer times are quite well described by the calculated result. Melnikov *et al.* observe that their magnetic signal goes to zero at about 1 ps, and use this as an estimate of the spin-relaxation time (denoted as τ_s^{Au} there). This value differs from the established spin relaxation time $T_1 = 515$ fs in gold as determined from transport measurements in the diffusive regime. In the calculated results, the T_1 value of 515 fs enters as a parameter via $\tau_{\mathrm{sf}} = 2T_1$ and yields a spin density that goes to zero at the same time as in the experiment. The calculation therefore provides a link between the ultrafast, optically excited/detected spin dynamics, and diffusive transport studies. Regarding the degree of agreement, we would like to add two remarks. First, the relative height of the extrema in the calculated spin-density dynamics can be influenced by making the excitation spin dependent, i.e., by having $J_+^0 \neq J_-^0$. This is likely the case in the experiment but including a spin dependent excitation would introduce a fit parameter, without qualitatively changing the results obtained from the macroscopic equations (1) and (2). Second, the calculation seems to lead to sharper extrema and smaller signals at longer times. Very likely, this is due to our neglect of energy relaxation processes because the energy

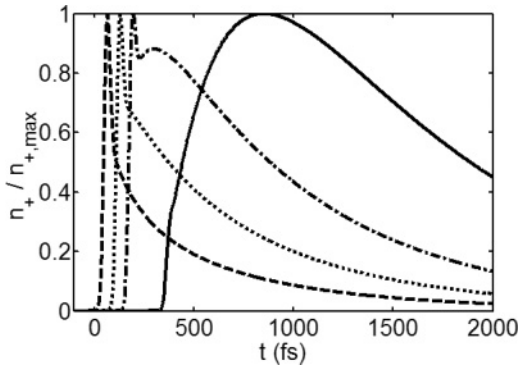

FIG. 8. Scaled dynamics of the density $n_+(z,t)$ of majority electrons at points $z = 50$ (dashed), 100 (dotted), 150 (dash-dotted), and 300 nm (solid) of an infinitely thick layer.

dependence of the distributions underlying the macroscopic equations is assumed to be essentially fixed and concentrated around the Fermi surface.[10] The last point is also important when comparing the charge dynamics in our Fig. 4(a) and Figs. 2(a) and 2(b) of Melnikov *et al*. The area under the calculated curves in Fig. 4(a) decreases strongly for larger values of L, whereas in the measurement it increases. In the calculation, this is a consequence of the spatial redistribution of the injected carrier density, as can be seen in Fig. 6(b). In the experiment, it is probably a result of the energy dependence of the nonlinear process that gives rise to the measured signal, and an energy redistribution of carriers during the dynamics. It is hard to say which is more important because a microscopic description of the SHG is quite involved.[29] To have a better comparison of the qualitative behavior of charge dynamics for the different slab thicknesses, we normalize the computed charge dynamics in Fig. 8. The normalization not only removes the difference in the peak heights, but also leads to a behavior at long times for both slab thicknesses that is very similar to the experimental result.

The spin and charge dynamics of our model based on a transition between ballistic and diffusive transport for one species of carriers is in agreement with Ref. 9 in that it emphasizes the importance of both ballistic and diffusive transport for the spin and charge dynamics. In contrast to our calculation, however, Ref. 9 stresses the energy dependence of the lifetimes of excited carriers and classifies *different* species of carriers, i.e., minority and majority electrons and holes, as contributing mainly to either ballistic or diffusive transport. From our results, it seems that the qualitative signatures of the observed dynamics are likely quite generic for transport in thin metal slabs on ultrashort time scales, regardless of the microscopic details, i.e., the energy dependence, of the excitation process and the subsequent relaxation dynamics.

Finally, we compare the general trends seen in Fig. 8 with an earlier measurement[26] of heat transport in thin gold films excited by a femtosecond laser pulse. This stretches the limits of the applicability of our calculation because in that experiment intraband excitation was likely dominant, leading only to a heating of the conduction electrons and not to an injection of carriers. However, the macroscopic equations for heat transport have the same mathematical properties as the ones used by us,[17,18] so that one can try to find indications of a qualitative agreement. In this case, we have to compare the normalized dynamics as shown in Fig. 8 because their Fig. 2 also shows normalized reflectivity changes. Indeed, the overall shape of the reflectivity changes observed by Brorson *et al*. match up well with our results. In particular, in Ref. 26 it is found "that the rise time of the signal increases slightly with increasing thickness." This trend is clearly observed in our calculated results and is explained by a change of dominantly ballistic dynamics in thinner samples to dominantly diffusive dynamics in thicker samples, here 300 nm. Importantly, this transition comes out of the calculation by a combination of ballistic and diffusive aspects; even in thicker samples where the diffusive dynamics dominates the rise time of the signal, there is still an important component of the result that can only be explained by ballistic dynamics, namely the delayed onset of the reflectivity response. As it was already noticed by Brorson *et al*., it is therefore hard to explain the observed rise times in terms of exclusively ballistic or exclusively diffusive transport. An analysis in terms of wave-diffusion dynamics removes the apparent contradiction between diffusive and ballistic properties of transport.

V. CONCLUSIONS

This paper presented an analysis of the wave-diffusion equations for spin and charge transport with special attention to the transition between ballistic and diffusive transport after ultrafast excitation. We showed that the wave character in Eqs. (1) and (2) is related to ballistic transport by analyzing the behavior of an analytical solution to these equations in one dimension. The simple, macroscopic equations work not only in the purely ballistic and diffusive limits, but can also be applied on time and length scales where spin and charge transport are neither completely ballistic nor diffusive.

Using the wave-diffusion equations, we modeled the conditions realized in a recent experiment in which spin-polarized electrons were excited in a gold film by optical pumping of an adjacent ferromagnetic layer and probed optically on the other side of the gold film. Under the assumption of slightly different relaxation times for spin-up and spin-down electrons, the simple macroscopic model qualitatively reproduced important signatures seen in the experiment, thus underscoring the importance of the transition between ballistic and diffusive transport for the observed dynamics. Because the model uses established macroscopic transport parameters and because the dependence of our results on one additional parameter, namely, the difference of the relaxation times, is extremely weak, our results are quite robust. This is an indication that the behavior observed in the experiment and shown by the calculated results is quite generic for ultrafast transport dynamics in thin metal films.

ACKNOWLEDGMENTS

We acknowledge support by the state of Rheinland-Pfalz through the MATCOR program and the MAINZ graduate school as well as by the Beijing Natural Science Foundation (No. 1112007).

*hcsch@physik.uni-kl.de

[1] Y. Tserkovnyak, A. Brataas, G. E. W. Bauer, and B. I. Halperin, Rev. Mod. Phys. **77**, 1375 (2005).

[2] S. O. Demokritov, B. Hillebrands, and A. N. Slavin, Phys. Rep. **348**, 441 (2001).

[3] M. W. Wu, J. H. Jiang, and M. Q. Weng, Phys. Rep. **493**, 61 (2010).

[4] J. Fabian, A. Matos-Abiague, C. Ertler, P. Stano, and I. Žutić, Acta Phys. Slov. **57**, 565 (2007).

[5] A. Mönnich, J. Lange, M. Bauer, M. Aeschlimann, I. A. Nechaev, V. P. Zhukov, P. M. Echenique, and E. V. Chulkov, Phys. Rev. B **74**, 035102 (2006).

[6] A. Kirilyuk, A. V. Kimel, and T. Rasing, Rev. Mod. Phys. **82**, 2731 (2010).

[7] E. Beaurepaire, J.-C. Merle, A. Daunois, and J.-Y. Bigot, Phys. Rev. Lett. **76**, 4250 (1996).

[8] M. Battiato, K. Carva, and P. M. Oppeneer, Phys. Rev. Lett. **105**, 027203 (2010).

[9] A. Melnikov, I. Razdolski, T. O. Wehling, E. T. Papaioannou, V. Roddatis, P. Fumagalli, O. Aktsipetrov, A. I. Lichtenstein, and U. Bovensiepen, Phys. Rev. Lett. **107**, 076601 (2011).

[10] Y.-H. Zhu, B. Hillebrands, and H. C. Schneider, Phys. Rev. B **78**, 054429 (2008).

[11] Y.-H. Zhu, B. Hillebrands, and H. C. Schneider, Phys. Rev. B **79**, 214412 (2009).

[12] T. Valet and A. Fert, Phys. Rev. B **48**, 7099 (1993).

[13] S. Zhang and P. M. Levy, Phys. Rev. B **65**, 052409 (2002).

[14] E. I. Rashba, Appl. Phys. Lett. **80**, 2329 (2002).

[15] J. Zhang and P. M. Levy, Phys. Rev. B **71**, 184417 (2005).

[16] Ł. Cywiński, H. Dery, and L. J. Sham, Appl. Phys. Lett. **89**, 042105 (2006).

[17] D. D. Joseph and L. Preziosi, Rev. Mod. Phys. **61**, 41 (1989).

[18] M. Chester, Phys. Rev. **131**, 2013 (1963).

[19] F. Steininger, A. Knorr, P. Thomas, and S. W. Koch, Z. Phys. B **103**, 45 (1997).

[20] G. H. Weiss, Physica A **311**, 381 (2002).

[21] D. V. Averin and K. K. Likharev, J. Low Temp. Phys. **62**, 345 (1986).

[22] A. Prociuk and B. D. Dunietz, Phys. Rev. B **82**, 125449 (2010).

[23] N. Tsuji, T. Oka, and H. Aoki, Phys. Rev. Lett. **103**, 047403 (2009).

[24] G. Stefanucci and C.-O. Almbladh, Phys. Rev. B **69**, 195318 (2004).

[25] V. V. Kruglyak, R. J. Hicken, M. Ali, B. J. Hickey, A. T. G. Pym, and B. K. Tanner, Phys. Rev. B **71**, 233104 (2005).

[26] S. D. Brorson, J. G. Fujimoto, and E. P. Ippen, Phys. Rev. Lett. **59**, 1962 (1987).

[27] Wen-C. Chiang, C. Ritz, K. Eid, R. Loloee, W. P. Pratt, and J. Bass, Phys. Rev. B **69**, 184405 (2004).

[28] The numerical values of $n_s(z,t)$ are twice as large as the ones in Fig. 4 because there is no carrier density "lost" to propagation outside the slab.

[29] G. Lefkidis and W. Hübner, Phys. Rev. Lett. **95**, 077401 (2005).